Case Studies in Construction Materials 14 (2021) e00494

Contents lists available at ScienceDirect

Case Studies in Construction Materials

journal homepage: www.elsevier.com/locate/cscm

Case study

Condition assessment of concrete and glass fiber reinforced polymer (GFRP) rebar after 18 years of service life

Sivakumar Ramanathan*, Vanessa Benzecry, Prannoy Suraneni, Antonio Nanni

Department of Civil, Architectural, Environmental Engineering, University of Miami, Coral Gables, FL 33146, United States

ARTICLE INFO

Article history:
Received 12 October 2020
Received in revised form 21 December 2020
Accepted 14 January 2021

Keywords:
GFRP
Concrete
Degradation
Durability
Electron microscopy
Horizontal shear strength
Bulk resistivity

ABSTRACT

Concrete and glass fiber reinforced polymer (GFRP) bar samples from an 18-year old repair project executed on an existing dry-dock were obtained by coring the dry dock in two regions. Several destructive and non-destructive tests were performed on both materials. Testing performed on the concrete showed substantial variability and clear evidence of damage occurring over the years. Further, there were significant differences in the concrete obtained from two different regions of the dock. The concrete was carbonated and chloride from seawater had penetrated significantly into its depth. The GFRP bars showed relatively lower variability in terms of test results. Electron microscopy and horizontal shear strength results suggest that the GFRP surface of the bars had suffered some damage, whereas the core had remained unaltered. These findings regarding limited damage to the GFRP, taken together with recent advances in GFRP production technology, support the notion that concrete reinforced with GFRP bars is an attractive alternative to conventional steel reinforced concrete for marine infrastructure applications.

1. Introduction

Use of steel reinforced concrete in environments with high chloride concentrations (such as coastal regions) can result in rapid and severe corrosion of the reinforcement [1]. The corrosion causes concrete spalling [2], compromises the integrity of the structure [3], and eventually leads to a reduction of the service life [4]. Frequent repairs and corrosion protection measures, which are costly and interrupt service, are then needed to maintain structural integrity [5]. Glass fiber reinforced polymer (GFRP) reinforcement, which is a non-corrosive composite material, can be an attractive alternative to steel bars to ensure long-term performance of concrete structures [6]. Studies have been carried out on the use of GFRP reinforcement in structural applications including in members such as slabs and beams [7–9]. Due to the low modulus of elasticity and different bond characteristics of GFRP rebars, structural capacity and deflection of members can be different from those with steel. However, potential issues can be overcome through design modifications and innovations [9–12]. Apart from the lack of corrosion-related issues, the light weight and high strength of GFRP rebars are advantages when compared to conventional steel. On the other hand, the lack of long-term testing data is a disadvantage. Another potential disadvantage is cost, as the initial cost of GFRP reinforcement per meter can be about double the cost of steel reinforcement of similar diameter [13]. Despite their somewhat higher initial cost, better performance and lower costs over the long-term have resulted in increasing use of GFRP-reinforced concrete, especially in marine environments [14]. As the technology is relatively new, not many studies are available regarding long-term field performance of GFRP-reinforced concrete [15].

* Corresponding author.
E-mail address: sxr1063@miami.edu (S. Ramanathan).

https://doi.org/10.1016/j.cscm.2021.e00494

Therefore, in the current study, the results of a condition assessment of concrete and GFRP reinforcement used for the external repair of a dry-dock after 18 years of service are reported.

Accelerated conditioning has generally been used to evaluate long-term GFRP performance [8,16,17]. Typical accelerated environments involve exposure of GFRP bars, either naked or embedded in concrete, to alkaline/saline solutions at relatively high temperatures, and subsequent monitoring of the property degradation [18,19]. For example, Al-Salloum et al. [17] and Khatibmasjedi et al. [18] have shown that exposure of GFRP to marine environment does not result in a significant loss of tensile strength of GFRP reinforcement. However, accelerated conditioning at a temperature of 60 °C (i.e., the highest temperature used in most studies and required by quality control provisions) has been suggested to overestimate GFRP deterioration. In addition, since the degradation of a composite is a complex physicochemical process, converting the results obtained under accelerated conditions to those under field exposure is non-trivial [20]. Current models used to predict long-term performance from accelerated testing methods under sustained loads do not accurately capture long-term behavior [21,22] since the negative effects of sustained loading on the tensile strength retention of GFRP reinforcement may be exacerbated at higher temperatures [23]. Therefore, there is a critical need to evaluate GFRP performance using specimens extracted from structures in service. A study on GFRP rebars embedded in concrete after 8 years exposure to harsh conditions including deicing salts and freezing and thawing showed limited degradation [24]. Gooranorimi and Nanni [25] studied the integrity of GFRP reinforcement extracted from a bridge deck in Texas after 15 years of service life; significant damage to the microstructure was not observed. Al-Khafaji et al. [26] studied the durability of GFRP extracted from different bridges (with a service life of 15–20 years) from across the US, including bridges exposed to freeze-thaw and deicing salts. Their conclusions were similar to those of others – damage to GFRP was extremely limited [26].

This study is an additional contribution to closing a gap in literature and to assessing, for the first time, the condition of GFRP bars in a structure exposed to marine environment after 18 years of service. Several tests are carried out on extracted samples to evaluate potential damage in both concrete and GFRP bars.

1.1. Structure background

Concrete cores containing GFRP bars were extracted from dry-dock no. 4 at Pearl Harbor in Oahu, Hawaii. The original structure for the dry-dock was built in 1942 for the US Navy with reinforced concrete walls of thickness 7.6–9.1 m [27]. The dry-dock walls significantly degraded over time and repairs were performed to the fascia in the early 1990s using steel reinforcement with a 50 mm thick concrete cover. Due to subsequent corrosion of the steel reinforcement used in the first repair (and the consequent delamination and spalling of the concrete), a need rose for additional repairs, which were executed and completed in 2001 by removing affected concrete and steel reinforcement and replacing them using concrete reinforced with GFRP bars [27]. The condition of the dry-dock fascia during the execution of the second round of repair is shown in Fig. 1, depicting the areas where the deteriorated concrete was removed. This picture also shows the approximate locations where the concrete cores were extracted 18 years later for this study.

The continual damage of the steel and the concrete is common in structures exposed to seawater. While in principle, numerous methods to mitigate corrosion can be undertaken, it is extremely challenging to prevent corrosion in the long-term in-situ. In this case, the constant chloride ingress (from the seawater) and the wetting and drying cycles resulting from dry-dock operations coupled with a relatively low concrete cover (50 mm) resulted in extensive steel corrosion (seen clearly in Figs. 1 and 2).

The 2001 repair was carried out by using a grid of GFRP bars held in place by GFRP dowels embedded in epoxy resin as the concrete reinforcement (as shown in Fig. 3). Rebars 9- and 12-mm in diameter (#3 and #4) were used for the straight elements and 9-, 12-, and 16-mm diameter (#3, #4, and #5) bars were used for the bends. Further details regarding the repair can be found in literature [27].

Cores were extracted in 2019 after the repaired dock had experienced 18 years of service. The numbers shown in yellow font in Fig. 1 correspond to the approximate locations where concrete cores were extracted. The cores at locations 1–8 (Region I) were intended to contain GFRP reinforcement and cores at locations 9–16 (Region II) were expected not to contain any GFRP reinforcement. Fig. 1 suggests that the fascia in Region I and Region II experienced different levels of deterioration, presumably as a result of different concrete mixtures or different exposure levels.

2. Methods

2.1. Coring and specimen preparation

In summer 2019, a total of 19 concrete cores, 102 mm in diameter, were extracted from the fascia of the dry-dock, the approximate locations of which are shown in Fig. 1. A more detailed representation of the core extraction locations and state of the fascia are not possible due to security concerns in place at the dry-dock as this is a Naval base. In fact, civilian personnel outside pre-authorized construction workers were not allowed on the base. The extracted cores were double sealed immediately after coring and placed in a sealed plastic bucket. The cores were then air lifted from the Naval base and then sent to the university laboratory for testing.

A significant challenge encountered during the coring process was that it was not possible to detect the position of either steel or GFRP rebars prior to coring, since the contractor did not have any reinforcement detection equipment. Detection of

Fig. 1. Dry-dock fascia photograph taken at the time of the repair (2001) also showing approximate locations of cores taken in 2019.

Fig. 2. Corroded steel reinforcement in an extracted cored specimen (Core #10 – Region II). The steel rebar is likely from the repairs done in the 1990s.

GFRP is currently not possible due to the lack of instrumentation capable of discerning non-metallic reinforcement. Because of this "blind" drilling, many cores (13 out of the 19) did not intersect any bar.

Details of the cores are presented in Table 1. While it was expected that cores from locations 1–8 should have contained GFRP reinforcement and cores at locations 9–16 should not, Table 1 shows that this is not the case. Cores #2, 3, 4, 8 (Region I) and cores #13,15 (Region II) contained GFRP. Core #1 (Region I) and cores #10, 14 (Region II) contained steel rebars. The only GFRP bars that were intersected were the #5 bent bars. The steel rebars were #7 (22-mm diameter) bars.

Fig. 3. Doweled GFRP reinforcement grid in the fascia of the dry-dock (Region II).

Table 1
Summary of core details and tests performed on each core.

Core number (Region)	Diameter (mm)	Height (mm)	GFRP size for each bar extracted	Length of each bar extracted (mm)	Tests on concrete*	Tests on GFRP*
1** (I)	101.6	127.0	–	–	A, B, C	
2 (I)	101.6	101.6	#5, #5	76.2, 12.7		J, L
3-1 (I)	101.6	152.4	#5, #5	88.9, 76.2	A, B, C, D, E, F, G	H, K, L
3-2 (I)	101.6	152.4	–	–	A, B, E, F, G	
4 (I)	101.6	203.2	#5	88.9	A, C, F, G	H, K
5 (I)	101.6	127.0	–	–		
6 (I)	101.6	152.4	–	–	A, B, C, D, F, G	
7 (I)	101.6	152.4	–	–	A, B, C, D	
8 (I)	101.6	152.4	#5, #5	63.5, 76.2	F, G	I, J, L
9-1 (II)	101.6	101.6	–	–	A, B, C, D, F	
9-2 (II)	101.6	177.8	–	–	A, C	
10** (II)	101.6	254.0	–	–	A, B, C, E	
11 (II)	101.6	127.0	–	–	A, B, C, D, F, G	
12 (II)	101.6	101.6	–	–	A, C	
13-1 (II)	101.6	101.6	#5, #5, #5	86.4, 83.8, 88.9	E, F	H, I, J, K
13-2 (II)	101.6	88.9	–	–	A, C, E, F, G	
14** (II)	101.6	127.0	–	–	A, B, C, E, F, G	
15 (II)	101.6	203.2	#5, #5	27.9, 76.2	A, C, E, F	I, J, L
16 (II)	101.6	127.0	–	–	A, B, C, E, F, G	

* Test labeling is as follows: A - Density, B - UPV, C - Bulk resistivity, D - Compressive strength, E - Splitting tensile strength, F -Chloride penetration, G - Carbonation depth, H - Fiber content, I - Water absorption, J - DSC, K - Horizontal shear strength, L - SEM/EDS. Tests A-G are on concrete and H-L are on GFRP.
** These cores had #7 steel rebars.

The cores received were not of "full" length but were broken into smaller pieces enabling multiple tests on each core. Further, the cores did not have a uniform length and had uneven end surfaces. An example core as received at the laboratory is shown in Fig. 4a. The surfaces of the cores were prepared by carefully cutting with a wet saw to obtain smooth end surfaces needed to carry out concrete testing, as shown in Fig. 4b. The cores (cores #1, 4, 10, 12, 13, 14, 15, and 16) did not have the desirable "standard" length (i.e., a 2 to 1 aspect ratio) before or after sample preparation. Finally, some cores (cores #2, 5, and 8) had a significant amount of macrovoids or extremely irregular end surfaces (which, if cut, would have led to specimen sizes that could not be tested). Such cores were used for measuring concrete carbonation depth and chloride penetration.

Some cores had steel reinforcement embedded in them (cores #1, 10, 14). Carbonation and penetration were tested on these cores since other tests, such as compressive strength or ultrasonic pulse velocity could not be performed. Because cores #1–8 and cores #9–16 appear to come from different regions possibly made with different concrete mixtures at different ages, analysis of results is performed by separating out data from the two subsets. The entire population data is also shown for completeness and for comparison.

The GFRP rebars were removed with the help of a metal spatula after cutting the concrete around it using a saw. The GFRP bars had been tied with the use of steel ties that were visually corroded. The GFRP bars were gently cleaned of any adhered concrete and cut with a water-cooled diamond abrasive wheel for specific sizes as required by the intended test.

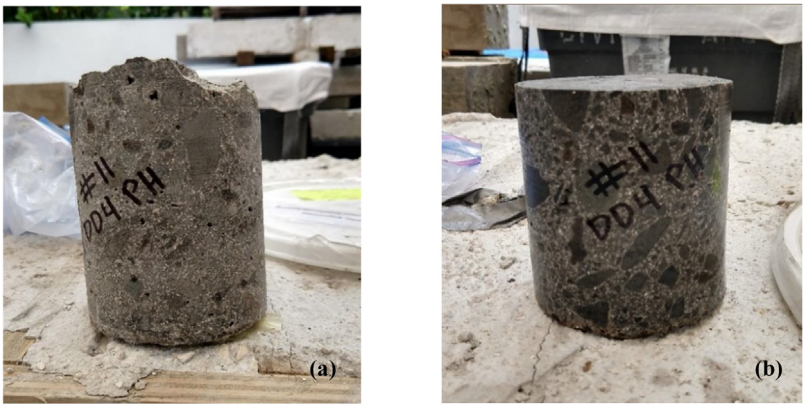

Fig. 4. Representative images of cores (a) as received, and (b) after preparing ends. (Core #11 – Region II).

2.2. Tests on concrete

2.2.1. Concrete density

The cores with the prepared surfaces were used to measure the as-received density of the concrete after surface drying. Since a standard ASTM method to measure as-received concrete density is unavailable, the procedure was adapted from UNE-EN 12390-7:2020. The as-received density gives an approximate estimate of the concrete quality and variability. The density is not affected by reinforcement as the measurement is performed after extracting the rebars and surface preparation. The coefficient of variation (COV) of measured values for all specimens was 9 %.

2.2.2. Ultrasonic pulse velocity

Ultrasonic pulse velocity (UPV) was performed in accordance with ASTM C597-16. UPV is non-destructive, simple, and has been reliably used as an indicator for assessing concrete quality and degradation [28]. After preparing the end surfaces, the specimens were gently dried to remove any moisture and allowed to surface dry before carrying out the test in the direct mode. A water-soluble gel was used as a coupling agent to ensure that there were no air gaps while carrying out measurements. The UPV values of specimens with a length/diameter ratio of less than 1.0 are not reported as these values may not be reliable [29]. Eight specimens were tested and the coefficient of variation of the measured values for all specimens was 15 %.

2.2.3. Bulk resistivity

Bulk resistivity testing was carried out using a resistivity meter at a frequency of 10 kHz based on ASTM C1876-19. Testing was carried out on specimens with an unknown degree of saturation and it is noted that the degree of saturation has a complex effect on the bulk resistivity [30]; therefore, interpretation of values is not trivial. Vacuum saturation is complex, can be potentially destructive for the specimens, and hence was not carried out (due to the limited number of specimens). A total of 16 cores were tested and corrections for specimen dimensions were applied based on Spragg et al. [31]. The COV of the measured values for all specimens was 31 %.

2.2.4. Compressive strength

After carrying out the non-destructive concrete tests, selected cores were tested for their compressive strength using a mechanical testing device in accordance with ASTM C39/C39M-18. Cores which had an aspect ratio (length/diameter ratio, L/D) of around 1.5 were tested. The concrete cylinders were capped with a sulfur cap and loaded at the rate of 15 $\pm$ 3 MPa/minute. Five specimens were tested in compression and a correlation strength factor was used for specimens with an L/D less than 1.75, based on ASTM C42/C42M-20. The COV of the measured strength values for all specimens was 30 %.

2.2.5. Splitting tensile strength

Splitting tensile strength test was carried out in accordance with ASTM C496/C496M-17 using a mechanical testing device. Six specimens with L/D $\leq$ 1 were tested at a loading rate of 0.7 MPa/minute. The COV of the measured splitting tensile strength values for all specimens was 32 %.

2.2.6. Chloride penetration and carbonation depth

The cores after compression and tensile testing were split in half and chloride penetration and carbonation depths were measured by spraying the split faces of the cores with 0.1 N silver nitrate (NT Build 492) and phenolphthalein (ACI 228.2R-13) respectively. A total of 12 cores were tested; one of the split faces was sprayed with silver nitrate and the other face was sprayed with phenolphthalein. Since the cores tested were not of full length, an exact depth of penetration from the surface cannot be

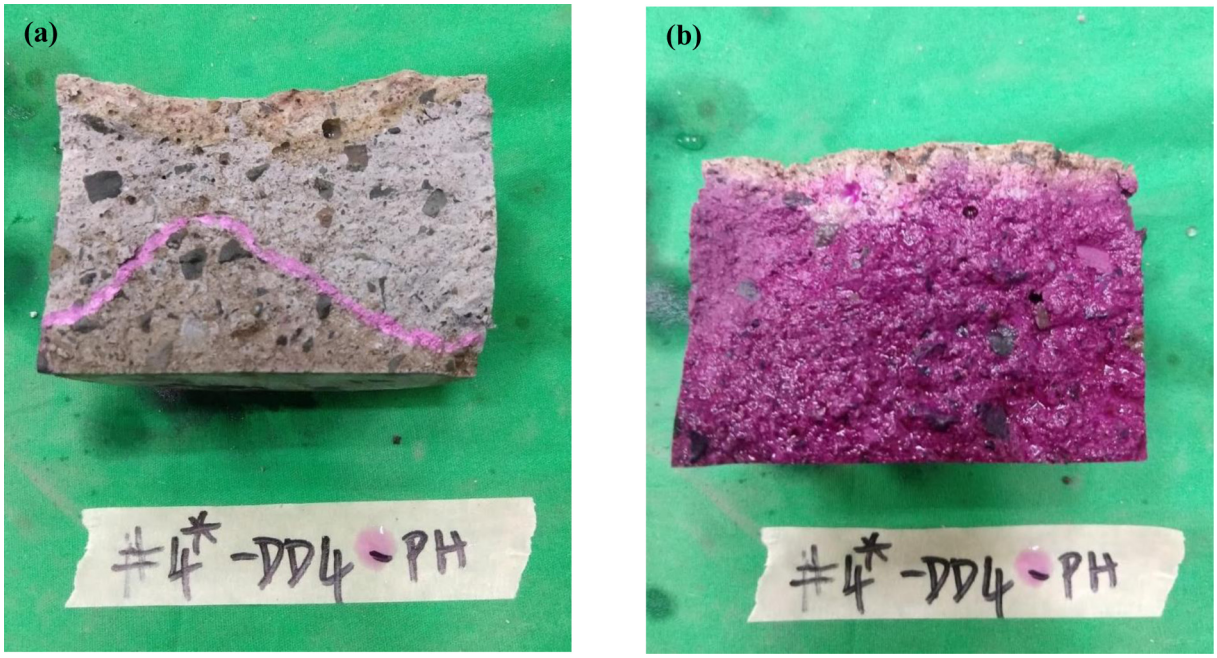

Fig. 5. Representative image of core tested for (a) chloride penetration, and (b) carbonation depth (Core #4 – Region I).

calculated without further details of the coring process. The values were measured for the respective cores using a Vernier caliper. Representative image showing measurement of chloride penetration depths and carbonation depth is shown in Fig. 5.

2.3. Tests on GFRP reinforcement

2.3.1. Fiber content

Fiber content testing was performed in accordance with ASTM D2584-18. Extracted GFRP rebar specimens 10 ± 1 g in weight were conditioned at 40 ± 2 °C and a relative humidity of 50 ± 10 % for 48 h. Ceramic crucibles were heated to 510 °C for 10 min in a muffle furnace to eliminate any combustible material from previous tests. The specimens and crucibles were then placed in a desiccator to cool to room temperature and then weighed using an analytical balance to record their initial weight. The specimens were placed in the ceramic crucibles and then inside the muffle furnace for the burn-off process. The burn-off process heated the specimens at a rate of 40 °C/min to 365, 450 and 700 °C for 50, 50 and 30 min, respectively. The ignited specimens and crucibles were removed and placed in a desiccator to cool down and weighted to record their final weight. The fiber mass fraction was calculated using the method described in ASTM D7957-17 and included the weight of possible fillers used in the resin. No effort was made to remove any remnant fillers in the resin or bar coating (such as sand particles and fiber wrap). Twelve specimens from four different extracted bars were tested to measure the fiber content and the COV of the measurements was less than 1 %.

2.3.2. Water absorption

Water absorption testing was performed in accordance with ASTM D570-98. GFRP rebar specimens of length 25 mm were conditioned by drying at 50 °C for 48 h in an oven. The specimens were then cooled to room temperature and weighed using an analytical balance. The conditioned specimens were then immersed in distilled water at 50 °C for 24 h. At the end of 24 h, the specimens were taken one at a time, dried using a paper towel and weighed using an analytical balance. This process was repeated a week later and then every two weeks until the increase in weight between two consecutive measurements was less than 1 %. A total of 6 specimens from two different bars were tested for water absorption and the COV of the equilibrium absorption values was 7 %.

2.3.3. Differential scanning calorimetry

Differential scanning calorimetry (DSC) was carried out on GFRP bar specimens prepared from the extracted bars. The bars were cut with a water-cooled diamond abrasive wheel into specimens of approximately 5 × 5 × 3 mm. The specimens were pre-conditioned by drying at 50 °C for 48 h in an oven. The specimens were tested according to the procedure described in ASTM E1356-08. The glass transition temperature (T_g) was determined from the change in slope on the DSC curves and compared with the requirements prescribed in ASTM D7957-17. DSC was performed on ten specimens from four different bars and the COV of the temperature was 15 %.

2.3.4. Horizontal shear strength

Horizontal shear strength was measured on the extracted GFRP bars in accordance with ASTM D4475-02. GFRP bar coupons of span length of approximately 50 mm (span-to-diameter ratio = 3) were center loaded. The ends of the specimen rested on supports that allowed the specimen to bend under load. Loading was applied at a rate of 1.3 mm/min. The specimen was loaded until shear failure occurred at the midplane of the bar cross section. Horizontal shear tests were performed on four bar coupons and the COV was 15 % for the specimens tested. No further mechanical testing was possible due to non-availability of GFRP specimens of suitable length.

2.3.5. Scanning electron microscopy with energy dispersive spectroscopy

Scanning electron microscopy (SEM) with energy dispersive spectroscopy (EDS) was performed on five specimens. The extracted GFRP specimens were cut and embedded in epoxy. Each specimen was polished using different silicon carbide grits levels and fine polishing was done using 3- and 1-μm diamond pastes. Prior to imaging, the specimens were gently dried using a cloth to remove residual moisture. The specimens were then sputter coated with gold to improve conductivity. SEM imaging was carried in the secondary electron mode at an accelerating voltage of 10 kV under high vacuum at a working distance of 10–12 mm. The specimens were imaged at different magnifications ranging from 100x to 1500x to capture morphological details. EDS were performed in the backscattered electron mode at an accelerating voltage of 15 kV under high vacuum for the same specimens. Imaging and EDS analysis were carried out on at least 20 different spots on each of the five specimens.

3. Results and discussion

3.1. Concrete

3.1.1. Density and UPV

Fig. 6 shows the range of density values for the specimens. For box and whisker plots, the crosses on either side represent the maximum and minimum values, the top and bottom sides of the box represent the upper and lower quartile values, the

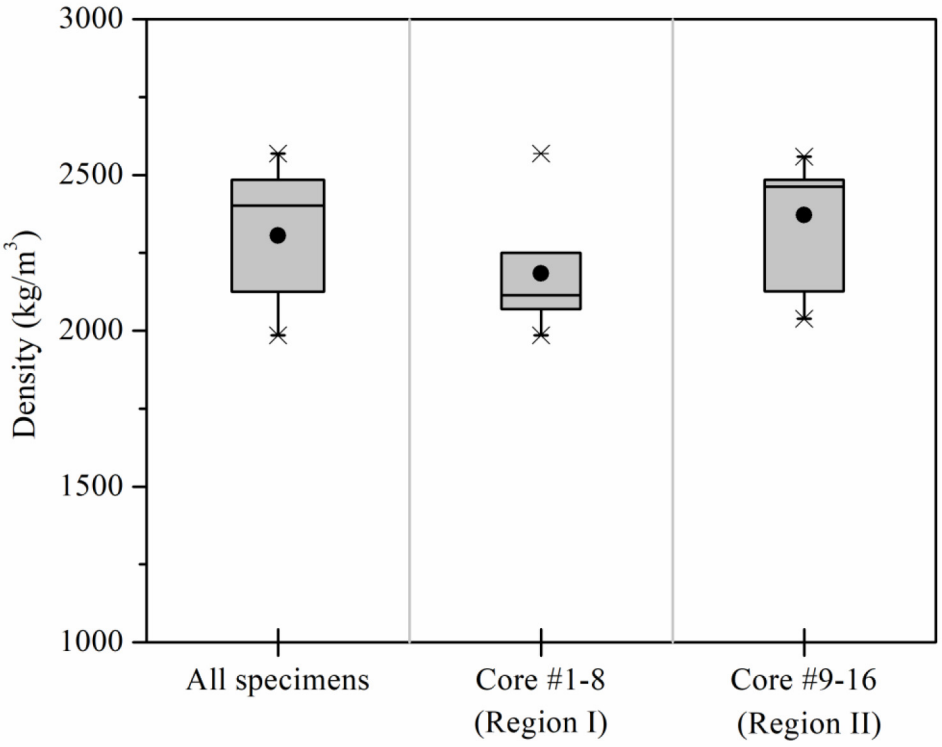

Fig. 6. Range of density values for the cores.

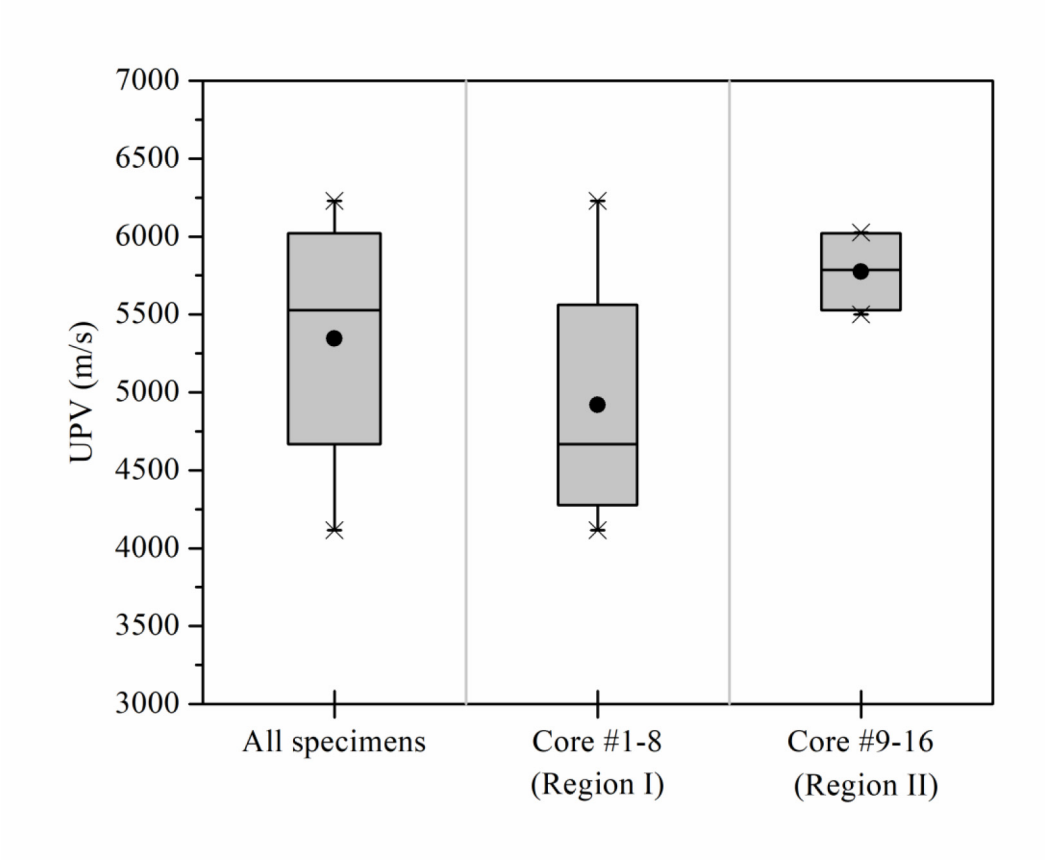

Fig. 7. Range of UPV values for the specimens.

line inside the box represents the median value, and the dot represents the mean value. This interpretation is valid for this and other box and whisker plots shown in the text.

The average density is 2305 kg/m^3 and the values range from 1985 to 2568 kg/m^3. The large range of density clearly shows the concrete variability. When specimens are grouped into those coming from Region I (cores #1-8) and Region II (cores #9-16), the spread in the data does not appear to be reduced. Specimens from Region II have an average density higher than those in Region I by 9 %. Low densities are an indicator of concrete damage during the service life due to cracking, leaching, or spalling, although they could also be due to differences in mixture design. Decrease in concrete density due to leaching of calcium has been observed in literature [32].

The UPV values (shown in Fig. 7) range from 4114 m/s to 6229 m/s with an average UPV value of 5347 m/s. These values are high; which is expected considering the concrete age. Interpretation of UPV in carbonated specimens with unknown saturation states is complex, but the range is further evidence of the concrete variability. The high values of the UPV suggest that the concrete quality is generally good [33,34], however, some portions of the structure, particularly Core #6 (UPV =4437 m/s) and Core #7 (UPV =4114 m/s), appear to have deteriorated, considering the lower UPV values. Visual inspection confirms this interpretation, and some concrete in this zone has spalled and cover concrete has been lost. It is not possible to further evaluate deterioration, considering the properties of the original concrete(s) are not known. Separating out data from Region I and Region II shows that the latter have a statistically higher UPV mean than the former. Cores from Region I appear to show a greater data range in the UPV measurements. High COV values are somewhat expected in field mixtures [35], and severe exposure tends to exacerbate variability.

The density and the UPV values strongly correlate, although the number of data points is somewhat limited. As the concrete density increases, the UPV value increases (Fig. 8). The explanation for this behavior is that ultrasonic waves travel faster through a denser medium compared to a less dense medium with pores and lower density [36,37]. Similar trends regarding concrete density and UPV have been observed in literature where there is a decrease in UPV values with a decrease in density of concrete [37]. The strong correlation seen here, combined with visual assessment, suggests that the lower density and lower UPV concrete is of poorer quality, likely due to damage, although lack of information regarding the original concrete prevents drawing further inferences.

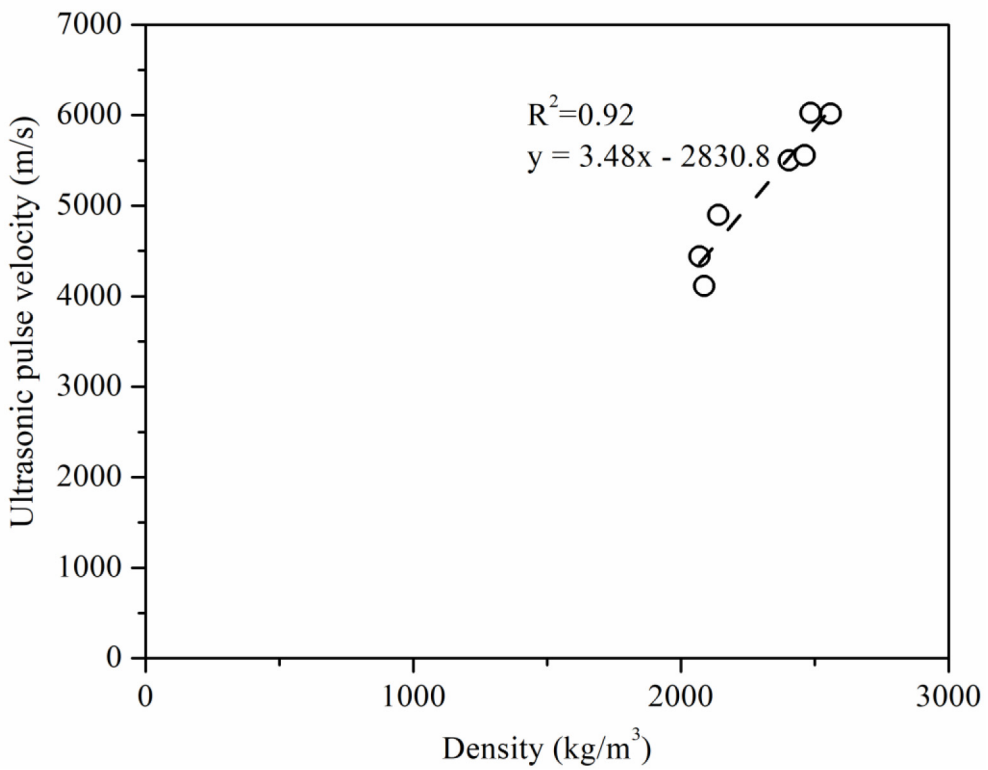

Fig. 8. Correlation between density and UPV values.

3.1.2. Bulk resistivity

Bulk resistivity values (shown in Fig. 9) of the concrete showed significant variation, ranging from 68 to 180 Ω-m, with an average bulk resistivity of 118 Ω-m and a standard deviation of 37 Ω-m for 16 specimens. Only five measurements were within 15 % of the mean value and four cores showed values greater than one standard deviation on the mean. While the actual mixture design for the concrete is unknown, it is possible that supplementary cementitious materials would have been used in the concrete mixture. If this assumption is true, the bulk resistivity values are significantly lower than what is expected for a concrete mixture at ages later than 10 years. Bulk resistivity values for concrete exposed to similar conditions typically range from 300 to 1000 Ω-m [38]. The lower bulk resistivity values suggest concrete deterioration, due to leaching and ingress of aggressive species such chlorides from the seawater. One must keep in mind that interpreting bulk resistivity values can be tricky in specimens of unknown degrees of saturation even in the lab and drawing conclusions for field specimens is therefore fraught with uncertainty. There does not appear to be a significant difference in the bulk resistivity values for cores from Regions I and II, when considering the data variability.

Bulk resistivity and UPV values for the same specimens show a moderate correlation (Fig. 10), likely because both measures are indicators of concrete quality. Good correlations have been observed in literature for UPV and bulk resistivity [39,40] for lab specimens. However, since the specimens have an unknown degree of saturation, the correlation is only moderate here.

3.1.3. Compressive and splitting tensile strength

Fig. 11a and b show the range of values for compressive and splitting tensile strengths of the concrete core specimens tested. The compressive strength shows significant variation and ranges from 26 to 55 MPa, with an average compressive strength of 42 MPa and COV of 31 %. In compression, cores from Region II show a statistically greater strength than cores from Region I (though note the limited number of specimens tested for Region II). The splitting tensile strength also shows significant variation, with values ranging from 3.5 to 6.3 MPa, with an average value of 4.4 MPa (COV of 32 %). Not enough specimens from Region I and Region II were tested to be able to compare the data in detail, though splitting tensile and compressive strength values did appear to correlate. The variations are significantly higher than what is expected from concrete mixtures in the lab but are to be expected from field mixtures with different levels of deterioration. The high COV values are consistent with the results from the other non-destructive test results. Since information regarding the initial design strength or the 28-day compressive strength of the concrete mixture is unavailable, no further analysis about deterioration can be made.

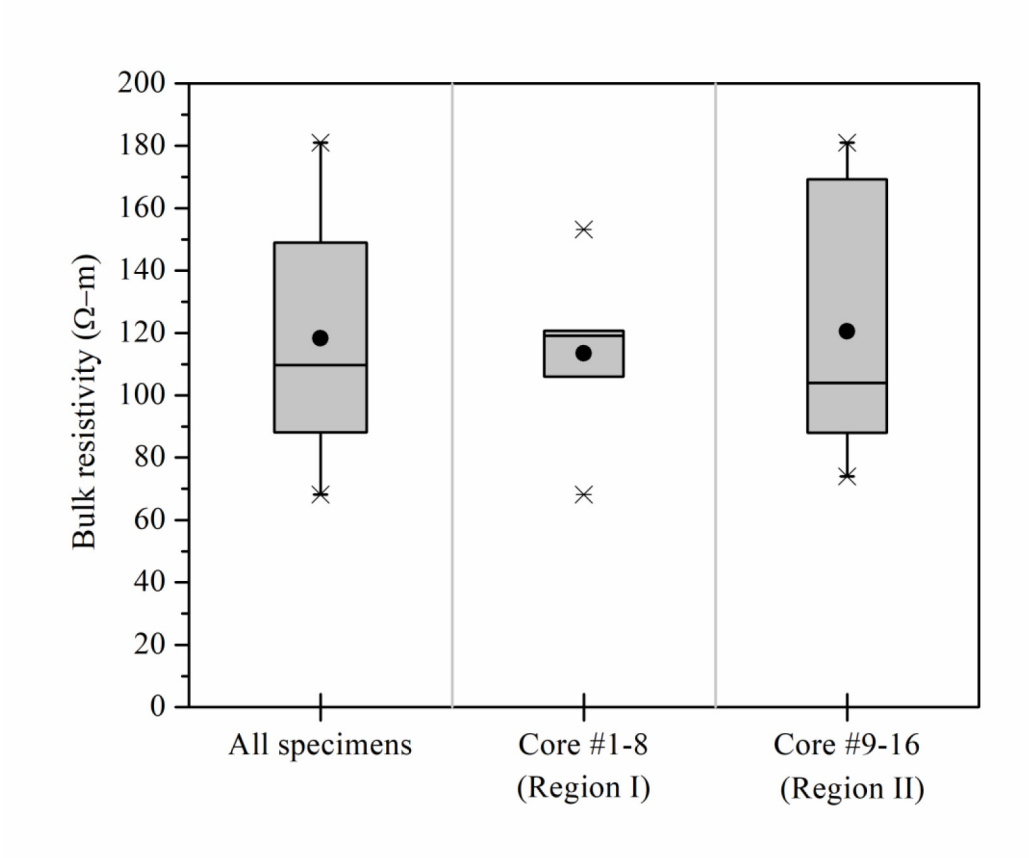

Fig. 9. Range of bulk resistivity values for the specimens.

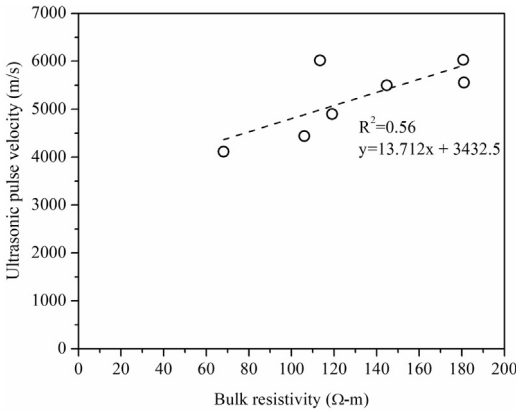

Fig. 10. Correlation between bulk resistivity and UPV.

A strong correlation is observed between compressive strength and the UPV values as seen in Fig. 12. Similar correlations between UPV and compressive strength have been shown in literature and the UPV values could be used to predict the compressive strength of concrete specimens. It has been suggested that theoretical equations [41,42] can be used to predict the compressive strength of field specimens based on UPV data. However, in this case, the UPV values predict that the compressive strength values should be significantly higher than what was observed. This discrepancy could be due to cracks induced in the concrete during specimen preparation (resulting in lower compressive strength measurements) or due to granitic aggregates (which can lead to higher UPV values [43]). The ultrasonic pulse velocity method is not sensitive enough to capture distributed microcracking in the matrix [44].

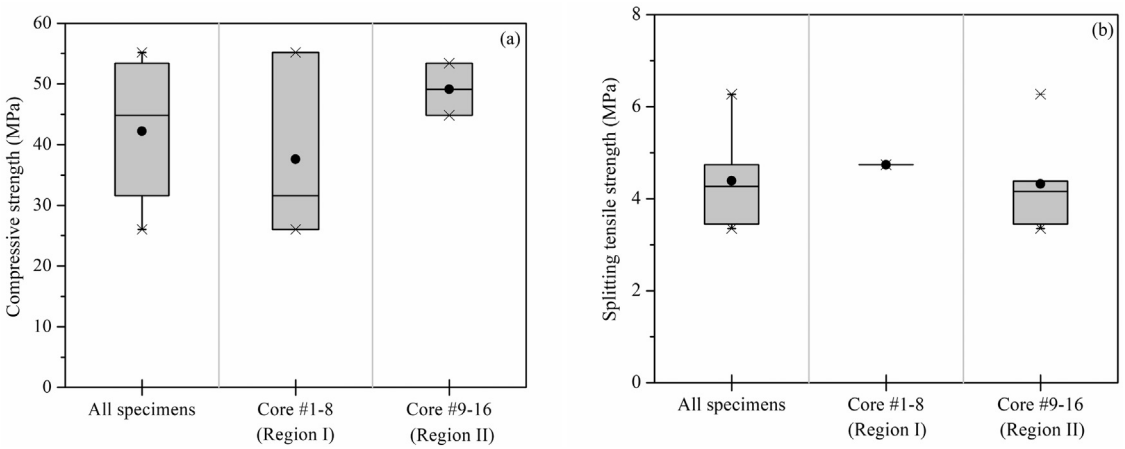

Fig. 11. Mechanical properties for the core specimens – (a) compressive strength and (b) splitting tensile strength.

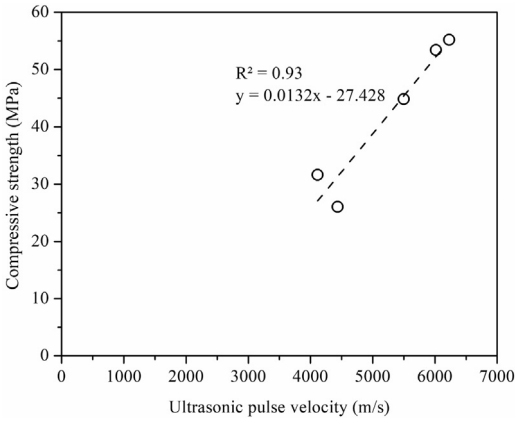

Fig. 12. Correlation between compressive strength and ultrasonic pulse velocity.

3.1.4. Chloride penetration and carbonation depth

Fig. 13a and b show the chloride penetration and carbonation depths for the core specimens tested. Since the depth at which the cores were obtained is not known, it is not possible to calculate the chloride penetration or carbonation depths

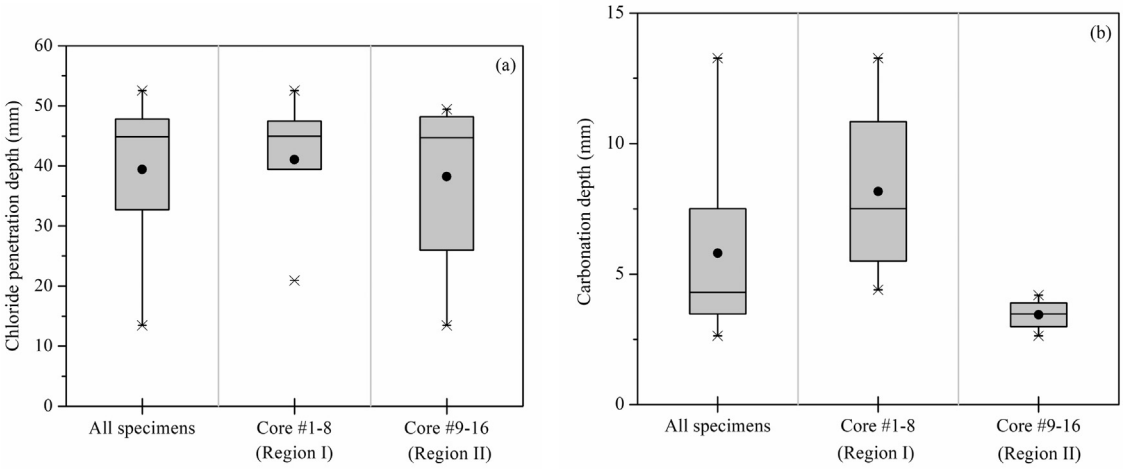

Fig. 13. Ingress of aggressive species (a) chloride penetration and (b) carbonation depths of the core specimens.

Table 2
Average, standard deviation (SD), and coefficient of variation (COV) of measured values shown for all data, for cores 1-8, and for cores 9-16. Units for all measures are given in the top row, COV is expressed as a percentage (– indicates the statistic could not be obtained due to limited number of samples tested).

Core #	Statistic	Density (kg/m^3)	UPV (m/s)	Bulk resistivity (Ω-m)	Compressive strength (MPa)	Splitting tensile strength (MPa)	Chloride depth (mm)	Carbonation depth (mm)
1-16	Average	2305.1	5347.1	118.3	42.2	4.4	39.4	5.8
	SD	207.5	784.2	37.1	12.3	1.1	12.5	3.6
	COV (%)	9.0	14.7	31.3	30.8	24.2	31.7	61.4
1-8	Average	2183.7	4919.5	113.4	37.6	4.7	41.1	8.2
(Region I)	SD	207.6	930.4	30.7	15.5	–	12.2	3.8
	COV (%)	9.5	18.9	27.1	41.2	–	29.8	46.2
9-16	Average	2371.4	5774.7	120.5	49.1	4.3	38.2	3.4
(Region II)	SD	183.5	285.9	40.8	–	1.2	13.5	0.6
	COV (%)	7.7	4.9	33.8	–	27.2	35.3	18.8

from the surface. The data presented here is qualitative and is only provided to present evidence of chloride penetration and carbonation, which are known to cause deterioration. The average chloride penetration depth is 39 mm with values ranging from 13 to 53 mm. Given that the cover depth is 50 mm on the fascia, and the chloride penetration depth is more than 50 mm in some locations, steel reinforcement in these regions has depassivated and corrosion has initiated [45]. This is confirmed visually in some cores (Fig. 2), where there is clear evidence of corrosion based on visual inspection. Some cores have "full" depth of chloride penetration. There does not appear to be an obvious difference in the chloride penetration behavior of cores from Regions I and II.

Similarly, there is considerable carbonation in the specimens, with the average depth of carbonation being 6 mm and the values ranging from 3 to 13 mm. Cores from Region I show a greater depth of carbonation than cores from Region II. The carbonation depth is lower than values reported in literature for field concrete at a similar age [25], presumably due to marine exposure causing higher chloride ingress than carbonation. However, as stated previously, since full cores were not received from the site, the depth of deterioration can be presented only for the individual cores and not for the structure itself.

3.1.5. Comparison of behavior of cores from region I and region II

Table 2 shows the average, standard deviation, and COV of measured values for all data, for cores from Regions I and II. When considering data for all cores, the COV values of many measurements are quite high, presumably due to the differences in the exposure conditions, damage, or differences in the concrete mixtures. When comparing Region I cores, Region II cores, and all data in terms of variability, the COV values are generally similar for each test, except for the UPV and carbonation tests. When comparing only the average values, it is apparent that Region II cores are of better quality than Region I cores. Region II cores have 9 % higher density, 17 % higher UPV, 6 % higher bulk resistivity, 31 % higher compressive strength, 7 % lower chloride penetration, and 59 % lower carbonation depth than Region I cores. On the other hand, the splitting tensile strength of cores from Region II is 9 % lower than the value observed for cores from Region I. While in some cases, the amount of data is limited, the fact that almost all measurements show a better performance for cores from Region II suggests that the concrete in cores 9-16 is of a better quality than the concrete in Region I cores (i.e. cores 1-8). This is likely due to different mixture design and/or different exposure. However, since information about the original concrete and coring process is limited, conclusions cannot be drawn with greater confidence.

3.2. Tests on GFRP reinforcement

3.2.1. Fiber content

The average fiber content of the bars was 75.4 %, which is higher than ASTM D7957-17 requirement of 70 % for such bars. The measured fiber content is higher than the original value for these bars, reported to be 73.6 %. This discrepancy could be due to the inclusion of concrete residues adhering to the bars (which would not present be on the pristine bar surface). It is also possible that the loss of some resin due to degradation in the aggressive aqueous environment could result in a higher fiber content compared to the pristine reinforcement. In any case, the fiber content values suggest that there is no significant fiber degradation after exposure to the harsh marine environment. This observation is consistent with literature, where it has been reported that GFRP specimens encased in concrete did not show significant fiber degradation [46], even under harsh exposure conditions.

3.2.2. Glass transition temperature

The average glass transition temperature is 90 °C, which is lesser than the current ASTM D7957-17 requirement of 100 °C. However, this value is typical of the glass transition temperature of GFRP reinforcement with vinyl ester resin manufactured about 20 years ago [47], although some literature shows higher values [24]. No further conclusions can be drawn regarding change of this property since the manufacturer data on pristine bars is not available

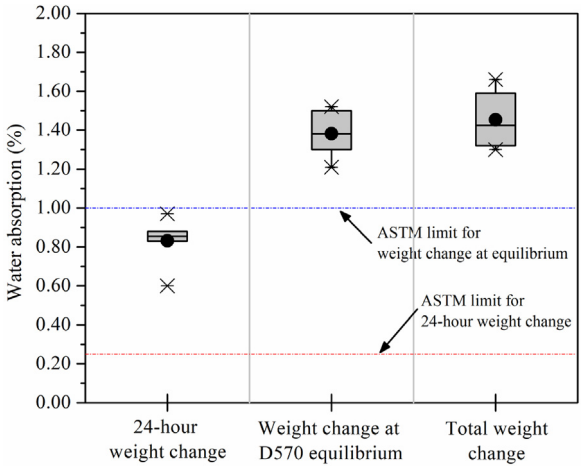

Fig. 14. Water absorption parameters for the GFRP specimens.

3.2.3. Water absorption

Fig. 14 shows the range of values obtained for the different water absorption parameters for the GFRP specimens. The 24 -h weight change due to water absorption ranges from 0.60 % to 0.97 %, with an average value of 0.83 %. The average weight change due to moisture absorption at equilibrium was 1.45 % with the values ranging from 1.30 to 1.66 %. These measured values are significantly higher than the ASTM D7957-17 limit of 0.25 % (for 24-h water absorption) and 1% (for weight change at equilibrium). These higher values could be because the GFRP bars used in this project were of older generation manufactured almost two decades prior to the publication of the ASTM specification. High water absorption may indicate deterioration of the matrix and debonding of the fiber. This debonding could cause an increase in the capillary uptake of moisture, resulting in increase in water absorption [48,49]. This deterioration, and the consequent increase in moisture uptake is consistent with literature and similar results for water absorption have been obtained in GFRP samples exposed to extreme environments such as increased temperature and sustained loading [46,50]. Water absorption can be considered an indicator of the quality of the matrix [50] and higher water absorption can be related to a reduction of the mechanical properties [51].

3.2.4. Horizontal shear strength

Fig. 15 shows the horizontal shear strength of the GFRP reinforcement after exposure. The results of horizontal shear strength from the original bars tested in 2001 after cure at ambient temperature and for bars post-cured at 100 °C for 12 h are also shown in Fig. 15. Some degradation in the horizontal shear strength after 20 years is apparent. Clear horizontal shear failure was observed in one of the four specimens tested, whereas failure of the other specimens presented as horizontal cracks on the outer surface in the region where loading was applied. Fiber debonding was observed in the cross section of

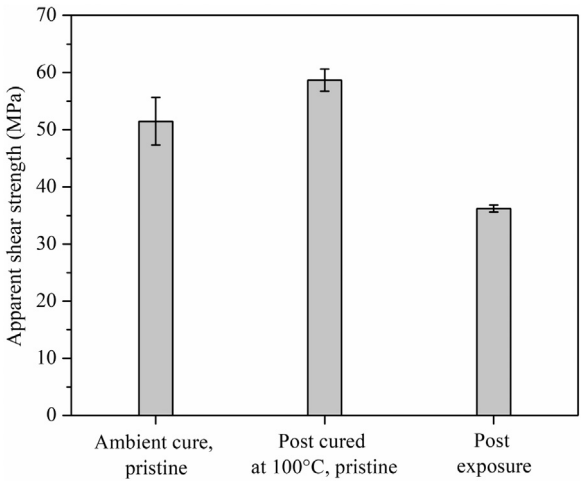

Fig. 15. Residual horizontal shear strength of the GFRP specimens.

some specimens. The debonding could be due to wetting and drying cycles experienced during the service life, resulting in shrinking and swelling of the matrix, weakening the interface between resin and fiber [48]. Imaging on other rebars appears to confirm some extent of fiber–to-resin debonding.

The decrease in apparent shear strength was 30 % and 38 % from ambient cured and post-cured bars prior to exposure, respectively. This reduction in strength could be due to various factors such as damage of resin [46], delamination between the resin and fibers [48], and the presence of voids in the fiber-resin interface [50]. The trend of decreasing shear strength with exposure to aggressive environment is generally similar to that observed in literature [18,52]. For instance, Khatibmasjedi et al. [18] reported a 27 % reduction in horizontal shear strength after exposure to a 60 °C alkaline solution over a 2-year period for similar GFRP bars made of E-glass fibers and vinyl-ester resin.

3.2.5. Scanning electron microscopy and energy dispersive spectroscopy

Fig. 16a–d shows representative SEM images of the fibers in the interior and near the skin of the GFRP specimens. No negatively affected fibers were observed on the interior of the bar cross-section. Damage near the bar surface is observed, which is described below. Some voids were observed near the skin of the bars, some of which could be a result of the manufacturing process, but based on horizontal shear strength reduction, they could also be due to the degradation in the fiber-resin interface. Some damaged fibers were observed where there was extensive degradation of resin (seen as voids in the SEM images). Long, continuous debonding cracks travelling towards the core of the specimens were observed in the resin-fiber interface. Debonding between the skin and the interior of the bars, characterized by large voids in the specimens, can be attributed to the wetting and drying cycles and the exposure to the harsh environment over the service life. Similar debonding was observed near the edge as a result of degradation in seawater by Khatibmasjedi et al. [18]. In some specimens, voids were observed closer to the center of the bar. This debonding between resin and fiber could explain the increased water absorption and reduction in apparent shear strength. Such debonding and voids could also explain the increased moisture uptake in the water absorption test. Similarly, a loss of bond at the interface has been observed by Mufti et al. [24]. The observations made here regarding GFRP reinforcing bars are similar to those presented in literature after accelerated testing and field exposure [23,53,54]. In general, the damage was not pervasive and was largely limited to the GFRP surface.

The results of EDS showed minimal presence of Na, Cl and K. The presence of Na was found in both the fiber and resin, and therefore is not an indication of chemical attack. The small amounts of Cl and K, on the other hand, were observed in the resin and could possibly indicate alkali attack. However, information from the original virgin bars would be necessary to confirm this interpretation.

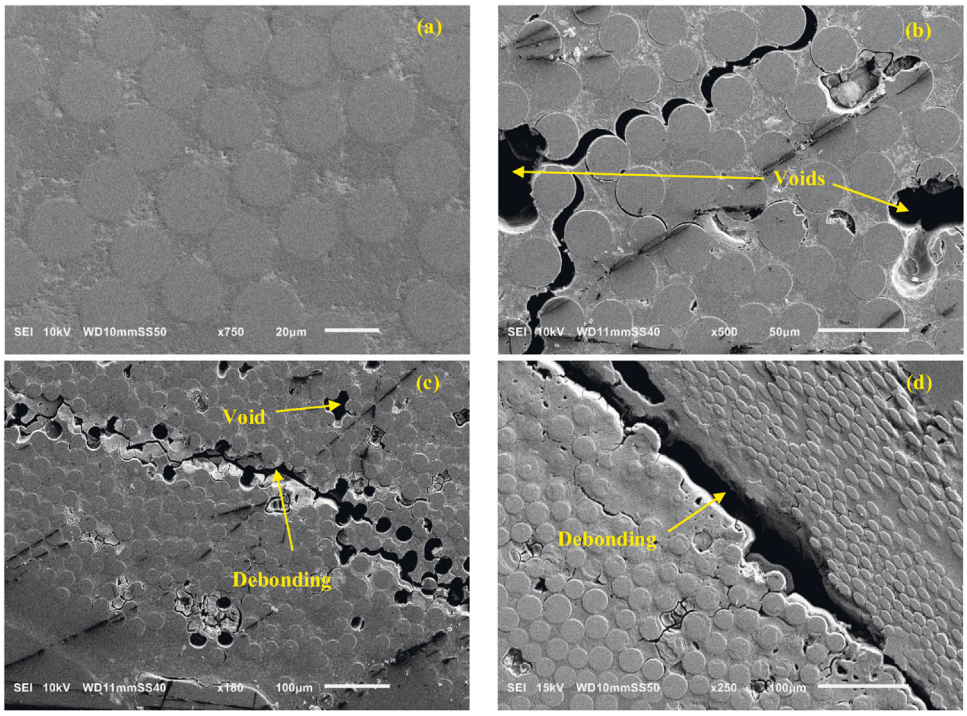

Fig. 16. SEM micrographs of GFRP reinforcement (a) interior of the bar, (b) debonding between resin and fiber, (c) missing fibers and resulting voids, and (d) debonding between the skin and the core of the bar.

4. Conclusions

Concrete and GFRP were cored from an 18-year old dry-dock and tested in detail. The major conclusions from the study are:

1 Measurements of concrete density, UPV, bulk resistivity, compressive strength, splitting tensile strength, chloride penetration, and carbonation depth all revealed significant variability, with COV values higher than 30 % for several tests.
2 Visual observations, low density, and significant variations in UPV, bulk resistivity, and strength values all suggest that the concrete was damaged. Further, concrete from cores #9-16 (Region II) appeared to show better performance than concrete from cores #1-8 (Region I) for almost all tests performed. It is not possible to determine exactly why these differences occur as mixture design data is unavailable, but these regions could have been made with different concrete mixtures and/or had different exposure conditions.
3 There was significant chloride penetration into the concrete; carbonation extent was not as high.
4 Fiber content, glass transition temperature, horizontal shear measurements, and scanning electron microscopy images did not show significant variability in the GFRP.
5 Water absorption and horizontal shear measurements suggested that some damage to the GFRP has occurred in the surface layer. Clear surface damage is observed in the scanning electron microscopy but significant damage to the GFRP core was not observed.

The lack of manufacturer data for the pristine GFRP reinforcement and the concrete mixture design is a significant impediment in studying the extent of degradation. The concrete appears to be extremely variable, and some specimens show clear signs of damage. The GFRP coupons show lesser variability, and some damage is evident from imaging and horizontal shear strength. While damage near the GFRP surface is extensive, the core of the bars still appears to be in good condition. The overall findings suggest that GFRP does not deteriorate significantly beyond the surface layer when embedded in concrete exposed to a marine environment for 18 years. This finding is line with the conclusions of other research groups who have studied GFRP degradation over roughly similar timeframes. The limited GFRP degradation does not cause volumetric expansion or substantial loss of section, as with steel. Therefore, this deterioration does not affect the service life significantly and members will not require extensive maintenance in contrast with structures containing corroding steel reinforcement. Considering that GFRP technology in terms of manufacturing and quality of constituents has improved substantially in the last 20 years, modern day GFRP reinforcement is expected to outperform the one used in this project.

Declaration of Competing Interest

The authors report no declarations of interest.

Acknowledgements

The authors would like to acknowledge both ACI Strategic Development Council and NSF I/U CRC Center for Integration of Composites into Infrastructure for their financial support. The financial support for the first author through the University of Miami Graduate School Dissertation Fellowship is gratefully acknowledged. The authors would also like to give credit for permitting and extraction of cores by CPI Foundation staff: Scott L. Burghardt, Steven Aguilar, Tanya W. Komas, Ph.D.; CPI Foundation active duty military Skillbridge team: SGT Morgan Kingston, SFC Corey Ray, LCPL Michael Acton, SGT Sebastian Angulo, SGT Dominic Barrera, PO2 Shawn Bartley, PO3 Jonathon Kammerer, SPC Michael Negron, CPL Kendrick Smith; U.S. Navy dry-dock engineering team: Perry Schneck, Russell Risch, Daniel Baba. Montale Tuen, undergraduate student at the University of Miami is thanked for his help with the testing of specimens. The authors would like to thank the reviewers for their insightful comments which helped in significantly improving the manuscript.

References

[1] D. Trejo, P.J. Monteiro, Corrosion performance of conventional (ASTM A615) and low-alloy (ASTM A706) reinforcing bars embedded in concrete and exposed to chloride environments, Cem. Concr. Res. 35 (2005) 562–571, doi:http://dx.doi.org/10.1016/j.cemconres.2004.06.004.
[2] J. Bilcik, I. Holly, Effect of reinforcement corrosion on bond behaviour, Proc. Eng. 65 (2013) 248–253, doi:http://dx.doi.org/10.1016/j.proeng.2013.09.038.
[3] C. Alonso, C. Andrade, J. Rodriguez, J.M. Diez, Factors controlling cracking of concrete affected by reinforcement corrosion, Mater. Struct. 31 (1998) 435–441, doi:http://dx.doi.org/10.1007/BF02480466.
[4] R.G. Pillai, et al., Service life and life cycle assessment of reinforced concrete systems with limestone calcined clay cement (LC^3), Cem. Concr. Res. 118 (2019) 111–119, doi:http://dx.doi.org/10.1016/j.cemconres.2018.11.019.
[5] P.H. Emmons, A.M. Vaysburd, Corrosion protection in concrete repair: myth and reality, Concr. Int. 19 (1997) 47–56.
[6] A. Younis, U. Ebead, S. Judd, Life cycle cost analysis of structural concrete using seawater, recycled concrete aggregate, and GFRP reinforcement, Constr. Build. Mater. 175 (2018) 152–160, doi:http://dx.doi.org/10.1016/j.conbuildmat.2018.04.183.
[7] H.F. Hassan, M.K. Medhlom, A.S. Ahmed, M.H. Al-Dahlaki, Flexural performance of concrete beams reinforced by GFRP bars and strengthened by CFRP sheets, Case Stud. Constr. Mater. 13 (2020)e00417, doi:http://dx.doi.org/10.1016/j.cscm.2020.e00417.
[8] C.N. Morales, G. Claure, A.R. Emparanza, A. Nanni, Durability of GFRP reinforcing bars in seawater concrete, Constr. Build. Mater. (2020)121492, doi:http://dx.doi.org/10.1016/j.conbuildmat.2020.121492.

[9] H.A. Abdalla, Evaluation of deflection in concrete members reinforced with fibre reinforced polymer (FRP) bars, Comp. Struct. 56 (2002) 63–71, doi:http://dx.doi.org/10.1016/S0263-8223(01)00188-X.
[10] H. Wang, A. Belarbi, Ductility characteristics of fiber-reinforced-concrete beams reinforced with FRP rebars, Constr. Build. Mater. 25 (2011) 2391–2401, doi:http://dx.doi.org/10.1016/j.conbuildmat.2010.11.040.
[11] E.M. Lotfy, S.M. Elzeiny, A.M. Rashad, Flexural capacity of one-way GFRP concrete slabs, Constr. Mater. 164 (2011) 143–152, doi:http://dx.doi.org/10.1680/coma.2011.164.3.143.
[12] M. Al-Rubaye, A. Manalo, O. Alajarmeh, W. Ferdous, W. Lokuge, B. Benmokrane, A. Edoo, Flexural behaviour of concrete slabs reinforced with GFRP bars and hollow composite reinforcing systems, Comp. Struct. 236 (2020) 111836, doi:http://dx.doi.org/10.1016/j.compstruct.2019.111836.
[13] T. Cadenazzi, G. Dotelli, M. Rossini, S. Nolan, A. Nanni, Cost and environmental analyses of reinforcement alternatives for a concrete bridge, Struct. Infra. Eng. 16 (2020) 787–802, doi:http://dx.doi.org/10.1080/15732479.2019.1662066.
[14] Z. Dong, et al., Durability test on the flexural performance of seawater sea-sand concrete beams completely reinforced with FRP bars, Constr. Build. Mater. 192 (2018) 671–682, doi:http://dx.doi.org/10.1016/j.conbuildmat.2018.10.166.
[15] F. Micelli, A. Nanni, Durability of FRP rods for concrete structures, Constr. Build. Mater. 18 (2004) 491–503, doi:http://dx.doi.org/10.1016/j.conbuildmat.2004.04.012.
[16] J.F. Davalos, Y. Chen, I. Ray, Long-term durability prediction models for GFRP bars in concrete environment, J. Comp. Mater. 46 (2012) 1899–1914, doi:http://dx.doi.org/10.1177/0021998311427777.
[17] Y.A. Al-Salloum, S. El-Gamal, T.H. Almusallam, S. H.Alsayed, M. Aqel, Effect of harsh environmental conditions on the tensile properties of GFRP bars, Comp. Part B: Eng. 45 (2013) 835–844, doi:http://dx.doi.org/10.1016/j.compositesb.2012.05.004.
[18] M. Khatibmasjedi, S. Ramanathan, P. Suraneni, A. Nanni, Durability of commercially available GFRP reinforcement in seawater-mixed concrete under accelerated aging conditions, J. Compos. Constr. 24 (2020) 04020026, doi:http://dx.doi.org/10.1061/(ASCE)CC.1943-5614.0001035.
[19] Y. Chen, J.F. Davalos, I. Ray, H.Y. Kim, Accelerated aging tests for evaluations of durability performance of FRP reinforcing bars for concrete structures, Compos. Struct. 78 (2007) 101–111, doi:http://dx.doi.org/10.1016/j.compstruct.2005.08.015.
[20] M. Robert, P. Cousin, B. Benmokrane, Durability of GFRP reinforcing bars embedded in moist concrete, J. Compos. Constr. 13 (2009) 66–73, doi:http://dx.doi.org/10.1061/(ASCE)1090-0268(2009)13:2(66).
[21] H.R. Hamilton, B. Benmokrane, C.W. Dolan, M.M. Sprinkel, Polymer materials to enhance performance of concrete in civil infrastructure, Poly. Rev. 49 (2009) 1–24, doi:http://dx.doi.org/10.1080/15583720802656153.
[22] H. Fergani, M. Di Benedetti, C.M. Oller, C. Lynsdale, M. Guadagnini, Long-term performance of GFRP bars in concrete elements under sustained load and environmental actions, Compos. Struct. 190 (2018) 20–31, doi:http://dx.doi.org/10.1016/j.compstruct.2018.02.002.
[23] H. El-Hassan, T. El-Maaddawy, A. Al-Sallamin, A. Al-Saidy, Performance evaluation and microstructural characterization of GFRP bars in seawater-contaminated concrete, Constr. Build. Mater. 147 (2017) 66–78, doi:http://dx.doi.org/10.1016/j.conbuildmat.2017.04.135.
[24] A.A. Mufti, N. Banthia, B. Benmokrane, M. Boulfiza, J. Newhook, Durability of GFRP composite rods, Concr. Int. 29 (2007) 37–42.
[25] O. Gooranorimi, A. Nanni, GFRP reinforcement in concrete after 15 years of service, J. Compos. Constr. 21 (2017) 04017024, doi:http://dx.doi.org/10.1061/(ASCE)CC.1943-5614.0000806.
[26] A.F. Al-Khafaji, R.T. Haluza, V. Benzecry, J.J. Myers, C.E. Bakis, A. Nanni, Durability assessment of 15–20 years old GFRP bars extracted from bridges in the USA—part 2: GFRP bar assessment, J. Compos. Constr. (2020) (Under review).
[27] A. Nanni, Relevant applications of FRP composites in concrete structures, Proceedings of the International Conference Composites in Construction–CCC2001, Porto, Portugal, 2001.
[28] F. Porco, G. Uva, A. Fiore, M. Mezzina, Assessment of concrete degradation in existing structures: a practical procedure, Struct. Eng. Mech. 52 (2014) 701–721, doi:http://dx.doi.org/10.12989/sem.2014.52.4.701.
[29] P. Wiciak, G. Cascante, M.A. Polak, Sensor and dimensions effects in ultrasonic pulse velocity measurements in mortar specimens, Proc. Eng. 193 (2017) 409–416, doi:http://dx.doi.org/10.1016/j.proeng.2017.06.231.
[30] H. Layssi, P. Ghods, A.R. Alizadeh, M. Salehi, Electrical resistivity of concrete, Concr. Int. 37 (2015) 41–46.
[31] R. Spragg, C. Villani, K. Snyder, D.P. Bentz, J.W. Bullard, W.J. Weiss, Factors that influence electrical resistivity measurements in cementitious systems, Transp. Res. Rec. 2342 (2013) 90–98, doi:http://dx.doi.org/10.3141/2342-11.
[32] Y.S. Choi, E.I. Yang, Effect of calcium leaching on the pore structure, strength, and chloride penetration resistance in concrete specimens, Nuc. Eng. Des. 259 (2013) 126–136, doi:http://dx.doi.org/10.1016/j.nucengdes.2013.02.049.
[33] R.S. Carcaño, E.I. Moreno, Evaluation of concrete made with crushed limestone aggregate based on ultrasonic pulse velocity, Constr. Build. Mater. 22 (2008) 1225–1231, doi:http://dx.doi.org/10.1016/j.conbuildmat.2007.01.014.
[34] L. Trifone, A Study of the Correlation Between Static and Dynamic Modulus of Elasticity on Different Concrete Mixes M.S. Thesis, West Virginia University, 2017. https://researchrepository.wvu.edu/etd/6833.
[35] C. Stergiopoulou, M.S. Aggour, R.H. McCuen, Nondestructive testing and evaluation of concrete parking garages, J. Infrastruct. Syst. 14 (2008) 319–326, doi:http://dx.doi.org/10.1061/(ASCE)1076-0342(2008)14:4(319).
[36] Z. Lafhaj, M. Goueygou, A. Dierbi, M. Kaczmarek, Correlation between porosity, permeability and ultrasonic parameters of mortar with variable water/cement ratio and water content, Cem. Concr. Res. 36 (2006) 625–633, doi:http://dx.doi.org/10.1016/j.cemconres.2005.11.009.
[37] J.A. Bogas, M.G. Gomes, A. Gomes, Compressive strength evaluation of structural lightweight concrete by non-destructive ultrasonic pulse velocity method, J. Ultras. 53 (2013) 962–972, doi:http://dx.doi.org/10.1016/j.ultras.2012.12.012.
[38] R.B. Polder, Test methods for on site measurement of resistivity of concrete—A RILEM TC-154 technical recommendation, Constr. Build. Mater. 15 (2001) 125–131, doi:http://dx.doi.org/10.1016/S0950-0618(00)00061-1.
[39] İ. Sertçelik, C. Kurtuluş, F. Sertçelik, E. Pekşen, M. Aşçı, Investigation into relations between physical and electrical properties of rocks and concretes, J. Geophy. Eng. 15 (2018) 142–152, doi:http://dx.doi.org/10.1088/1742-2140/aa87ca.
[40] M.B.H.A. Manaf, et al., Surface resistivity and ultrasonic pulse velocity evaluation of reinforced OPC concrete and reinforced geopolymer concrete in marine environment, Advances in Mechatronics, Manufacturing, and Mechanical Engineering, Singapore, (2020), doi:http://dx.doi.org/10.1007/978-981-15-7309-5_29.
[41] K.B. Sanish, M. Santhanam, Characterization of strength development of concrete using ultrasonic method, 18th World Conference on Non-Destructive Testing, Durban, South Africa, 2012.
[42] H.Y. Qasrawi, Concrete strength by combined non-destructive methods simply and reliably predicted, Cem. Concr. Res. 30 (2000) 739–746, doi:http://dx.doi.org/10.1016/S0008-8846(00)00226-X.
[43] A. Lorenzi, F.T. Tisbierek, L.C.P. Silva, Ultrasonic pulse velocity anályis in concrete specimens, IV Conferencia Panamericana De END, Buenos Aires, Argentina, 2007.
[44] S.F. Selleck, et al., Ultrasonic investigation of concrete with distributed damage, ACI Mater. J. 95 (1998) 27–36, doi:http://dx.doi.org/10.14359/349.
[45] D. Trejo, R.G. Pillai, Accelerated chloride threshold testing: Part I—ASTM A 615 and A 706 reinforcement, ACI Mater. J. 100 (2003) 519–527, doi:http://dx.doi.org/10.14359/12959.
[46] H. EL-Hassan, T. El Maddawy, Microstructure characteristics of GFRP reinforcing bars in harsh environment, Adv. Mater. Sci. Eng. 2019 (2019), doi:http://dx.doi.org/10.1155/2019/8053843.
[47] B. Benmokrane, O. Chaallal, R. Masmoudi, Glass fibre reinforced plastic (GFRP) rebars for concrete structures, Constr. Build. Mater. 9 (1995) 353–364, doi:http://dx.doi.org/10.1016/0950-0618(95)00048-8.
[48] F. Ceroni, E. Cosenza, M. Gaetano, M. Peccea, Durability issues of FRP rebars in reinforced concrete members, Cem. Concr. Compos. 28 (2006) 857–868, doi:http://dx.doi.org/10.1016/j.cemconcomp.2006.07.004.

[49] L. Prian, A. Barkatt, Degradation mechanism of fiber reinforced plastics and its implications to prediction of long-term behavior, J. Mater. Sci. 34 (1999) 3977–3989, doi:http://dx.doi.org/10.1023/A:1004647511910.
[50] B. Benmokrane, A.H. Ali, H.M. Mohamed, A. ElSafty, A. Manalo, Laboratory assessment and durability performance of vinyl-ester, polyester, and epoxy glass-FRP bars for concrete structures, Compos. Part B: Eng. 114 (2017) 163–174, doi:http://dx.doi.org/10.1016/j.compositesb.2017.02.002.
[51] L. Bian, J. Xiao, J. Zeng, S. Xing, Effects of seawater immersion on water absorption and mechanical properties of GFRP composites, J. Compos. Mater. 46 (2012) 3151–3162, doi:http://dx.doi.org/10.1177/0021998312436992.
[52] M.A. Sawpan, Shear properties and durability of GFRP reinforcement bar aged in seawater, J. Poly. Test. 75 (2019) 312–320, doi:http://dx.doi.org/10.1016/j.polymertesting.2019.02.033.
[53] F. Guo, S. Al-Saadi, R.K.S. Raman, X.L. Zhao, Durability of fiber reinforced polymer (FRP) in simulated seawater sea sand concrete (SWSSC) environment, Corr. Sci. 141 (2018) 1–13, doi:http://dx.doi.org/10.1016/j.corsci.2018.06.022.
[54] O. Gooranorimi, W. Suaris, E. Dauer, A. Nanni, Microstructural investigation of glass fiber reinforced polymer bars, Compos. Part B: Eng. 110 (2017) 388–395, doi:http://dx.doi.org/10.1016/j.compositesb.2016.11.029.